Schottky Barrier Catalysis Mechanism in Metal-Assisted Chemical Etching of Silicon

Ruby A. Lai,[†,‡] Thomas M. Hymel,[†,§] Vijay K. Narasimhan,[§,⊥] and Yi Cui*[,#]

‡Department of Physics, Stanford University, 382 Via Pueblo, Stanford, California 94305, United States
§Department of Materials Science and Engineering, Stanford University, 476 Lomita Mall, Stanford, California 94305, United States
#Stanford Institute for Materials and Energy Sciences, SLAC National Accelerator Laboratory, 2575 Sand Hill Road, Menlo Park, California 94025, United States

Ⓢ *Supporting Information*
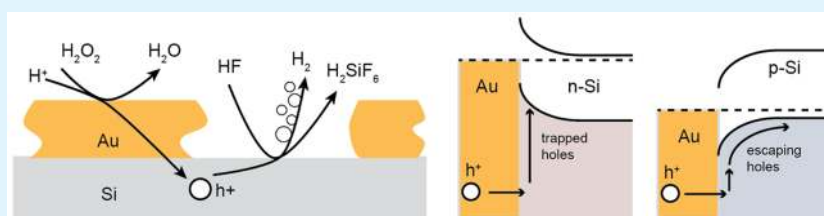
ABSTRACT: Metal-assisted chemical etching (MACE) is a versatile anisotropic etch for silicon although its mechanism is not well understood. Here we propose that the Schottky junction formed between metal and silicon plays an essential role on the distribution of holes in silicon injected from hydrogen peroxide. The proposed mechanism can be used to explain the dependence of the etching kinetics on the doping level, doping type, crystallographic surface direction, and etchant solution composition. We used the doping dependence of the reaction to fabricate a novel etch stop for the reaction.

KEYWORDS: metal-assisted chemical etching, nanoporous catalyst, reaction mechanism, anisotropic etching, kinetic rate exponents, dopant etch stop

Deep, patterned, anisotropic, high-aspect ratio silicon etching is of interest for semiconductor device processing, with potential applications for MEMS,[1] 3D transistors,[2] photovoltaics,[3,4] and batteries.[5] Metal-assisted chemical etching (MACE) is an example of a recently developed anisotropic electrochemical corrosion reaction.[6] Unlike other anisotropic wet etches like KOH, where the anisotropy relies on the etch rate suppression of one crystal face relative to another, features etched by MACE are not constrained by their crystallographic orientation, making high-aspect-ratio structures facile.[7] As a wet etch, MACE has the potential to be lower cost than deep reactive ion etching techniques like the Bosch process[7] that require vacuum, high frequency electronics, and ion optics. MACE has also been used to generate high surface area porous Si for diverse applications in optoelectronics, chemical sensing,[8] drug delivery,[9] and micromachining.[10]

MACE is characterized by the presence of an oxidant (such as H_2O_2, HNO_3, $KMnO_4$, or $HClO_4$), whose reduction is catalyzed by a metal (such as Au, Ag, Pd, Pt, Cu, or Ir, in the form of a deposited film or nanoparticles formed in situ).[3,11,12] The charge carriers (holes) generated by this half-reaction then participate with another reactant to dissolve the material by an oxidative etching half-reaction. MACE reactions for Si, GaAs, GaN, Ge, $Si_{1-x}Ge_x$, and SiC have all been demonstrated.[13] MACE of silicon stands out from other anisotropic Si etches by its lack of reliance on crystal axis. Features etched into a silicon wafer using MACE can be steeply vertical, no matter the crystal

surface orientation of the wafer. MACE can be applied for silicon micromachining at a range of scales, from millimeter to nanometer scales (Figure S1). In certain conditions, etching occurs only directly underneath a patternable metal catalyst,[14,15] which offers great spatial control. In other etching conditions, a porous Si surface is produced everywhere near the catalyst.[16,17] Despite its importance, the MACE mechanism is not fully understood.

In this paper, we propose a new understanding of the MACE mechanism in silicon, which explains previously observed but unexplained dependences of the etch rate on the silicon doping. We show that the catalyst metal film on the silicon plays a dual catalytic role in the MACE reaction. Previously, the metal had been understood to only catalyze the oxidative half-reaction. Here we propose an additional function of metal: forming a Schottky junction with Si to control the spatial distribution of the injected holes. The Schottky barrier band-bending formed on n-type silicon traps injected holes at the surface, promoting the oxidation of Si and speeding up etching. The band-bending is reversed in p-type silicon, which slows the oxidation and etching of Si by pulling holes away from the surface. The proposed mechanism can be used to explain the dependence of the etching kinetics on the doping level, doping type,

A

crystallographic surface direction, and etchant solution composition. We expect that this understanding can be generalized to develop other anisotropic solid corrosion reactions for compatibility with MEMS, integrated circuit, and solar cell manufacturing.

In our MACE system, hydrogen peroxide (H_2O_2) is catalytically reduced by a gold catalyst film, and a hole (h^+) is injected from the gold into the silicon. The oxidized silicon then etches by reaction with hydrofluoric acid (HF) to form a soluble silicon hexafluoride (Figure 1a).

$$H_2O_2 + 2H^+ \xrightarrow{Au} 2H_2O + 2h^+$$

$$Si + 4HF_2^- + 2h^+ \rightarrow SiF_6^{2-} + 2HF + H_2(g)$$
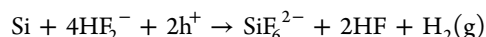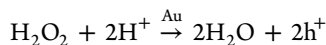
Following the methods of ref 18, our catalyst film is nanoporous, with pores with widths of about 10 nm, which allows access of the hydrofluoric acid to the silicon surface (Figure 1b). The nanoporous etching regime is distinct from but similar to the solid film regime.[16,18] We achieve this nanoporous morphology by electron evaporation of a 16 nm layer of Au without an adhesion layer. Throughout the reaction, the gold maintains an intimate electrical contact with the silicon, sinking with the silicon as it is etched. Because hole injection can take place only catalytically, in some cases the silicon etches only directly underneath the Au catalyst film and high anisotropy can be achieved. In this work, we have achieved an anisotropy ratio as high as 100 for n-type Si of $1-10$ Ω cm resistivity. The anisotropic etching also allows facile measurement of etch rates, which we have used here to elucidate new aspects of the MACE mechanism.

We measured the etch rate for a range of doping levels for both n-type and p-type (100) silicon across a range of solution concentrations (Figure 1c). N++, N+, and N are n-type silicon with resistivity $0.001-0.01$, $0.01-0.1$, and $1-10$ Ω cm, respectively, with P++, P+, and P similarly defined for p-type silicon. Sixteen nanometers of Au catalyst film was evaporated onto photolithographically patterned wafers with 5 μm wide lines spaced by 20 μm. We used an etchant solution with combined concentration of $C = [HF] + [H_2O_2] = 4.8$ M, and varied the proportion of HF, $\rho = [HF]/([HF]+[H_2O_2])$. The etch rate used throughout this paper refers to the vertical depth per unit time that the silicon is etched, or if the catalyst did not sink vertically, to the path length of the etching catalyst film. We show examples of the morphology of the etched silicon as a function of doping and solution (Figure 1d). See Figure S2a for a complete set of morphologies.

From the etch rates (Figure 1c), we observe the following trends, which cannot be explained by previously described heuristics of this reaction. First, although the etching half-reaction is mediated by holes, n-type silicon consistently etches faster than the hole-rich p-type silicon. Second, N, N+, and N++ etch rates are all very similar across this range of MACE etchant composition, despite the large differences in resistivity and hole concentrations. Third, the P++ etch rate is comparatively very low, while P and P+ etch rates are very similar.

To explain these observations on the etch rate, we consider how the doping of the silicon changes $[h^+]$, the concentration of holes available to react at the surface, at a fixed etchant composition. The energy levels of the oxidative and reductive half-reactions of MACE show that the hole is injected deep in the Si valence band (Figure 2a).[12] A Schottky barrier interface
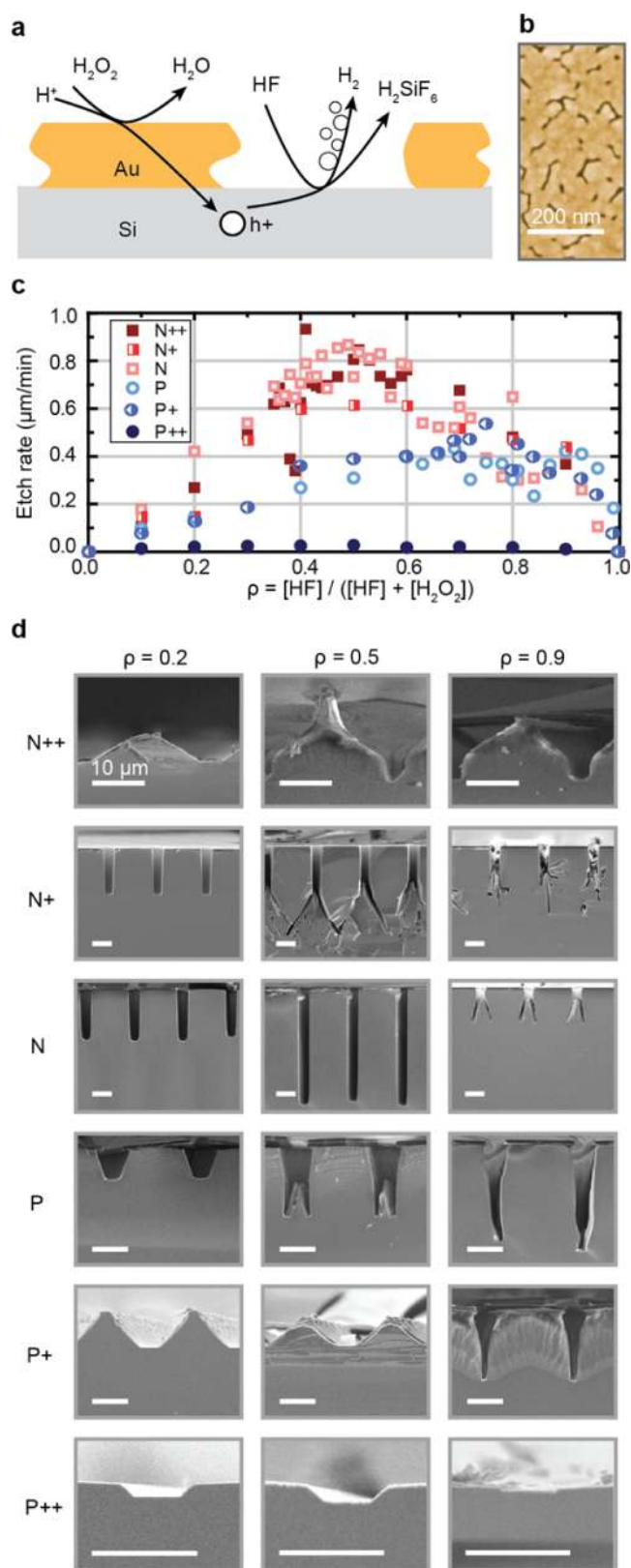

Figure 1. (a) Schematic of MACE silicon etching reaction. (b) False-color SEM of 16 nm nanoporous Au catalyst film. (c) Etch rate as a function of proportion of HF, $\rho = [HF]/([HF]+[H_2O_2])$, with a fixed combined concentration $C = [HF]+[H_2O_2] = 4.8$ M. N and P refer to the doping type of silicon and '+' means more highly doped. (d) SEM images of the silicon etched for 1 h. All scale bars are 10 μm.
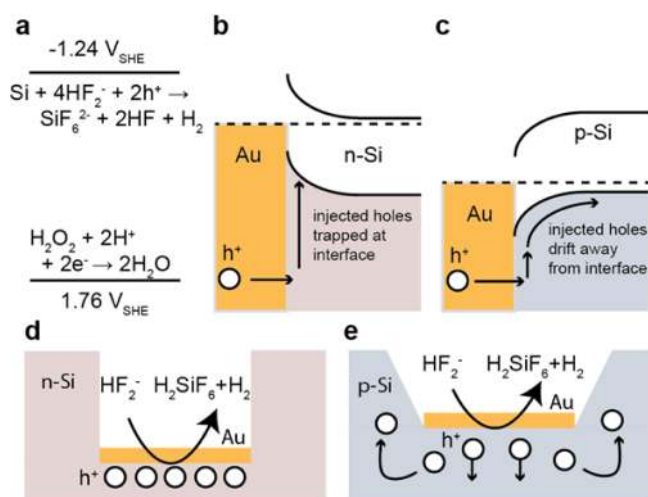
Figure 2. (a) Schematic of reduction potentials of the two MACE half-reactions relative to the standard hydrogen electrode, V_{SHE}. (b, c) Band-diagram of Au−Si interface for n-type and p-type Si, respectively, showing the behavior of hole carriers injected by the reduction of H_2O_2. (d, e) Schematic of the resulting morphology of MACE for n-type and p-type Si, respectively.

electric field between Au and Si confines holes to the surface for n-type Si (Figure 2b) and pulls holes away from the surface for p-type Si (Figure 2c), as observed also in metal-assisted anodic etching of silicon.[19] Thus, despite the higher concentration of holes in p-type silicon, holes are not available to react with the HF at the surface, so p-type silicon etches slower than n-type silicon.

We note that this band picture is valid because the Au maintains intimate electrical contact with the Si throughout etching. The Schottky barrier heights were measured using an $I–V$ technique (Figure S4).[20] The p-type Si shows a positive Schottky barrier height (from 0.5 to 0.8 eV), whereas n-type Si has a negative barrier height (from −0.5 to −0.8 eV). The sign and value of the measured Schottky barriers are consistent with literature values.[21,22]

Second, because the holes are confined near the surface in n-type Si, the surface is saturated with holes for N, N+, and N++ Si, so the reaction rates are all similar, despite the differences in doping.

Third, in p-type Si, the concentration of holes depends on the drift velocity of the holes away from the junction, which depends on the mobility and the electric field at the interface. We can estimate the drift velocity of holes based on well-known dependences among Si mobility, doping concentration and resistivity. The drift velocity is about 1×10^7, 2.5×10^7, and 1×10^8 cm/s for P, P+, and P++, respectively. Because mobility decreases and electric field strength increases with increased doping, P and P+ have very similar drift velocities and etch rates. However, for P++, the electric field strength overcomes the reduction in mobility: holes drift so quickly from the junction that they are unable to react, and the etch rate is slow.

The model also explains the etch morphology. For N and N+ silicon, because the holes are confined to the Au−Si junction, the etch is highly anisotropic (Figure 2d). With more highly doped N++ silicon, the Schottky junction width is small enough for carrier tunneling, so the etch occurs everywhere in a porous fashion (Figure 1d, N++, Figure S2b). In contrast, in p-type silicon, the injected holes drift away from the junction (Figure 2e). These holes can diffuse to the sidewalls of the

exposed Si trench, and the silicon etches there, thus widening the etched trench at the top (Figure 1d, P, P+, P++). The widening occurs more severely for P++ than P+ and P, because the holes drift away from the junction more quickly.

The fracture of the catalyst seen under some conditions has been observed previously, and has been explained by differences in spatial hole concentration.[23] For N++ and P+ Si, MACE etching forms thick layers of porous Si, as previously observed.[6] At extremely high [HF], we observe the formation of vertical silicon whiskers, also previously observed.[13] Higher ρ correlates with higher anisotropy: the faster HF reacts with injected holes, the less the holes are able to diffuse away from the metal catalyst, eventually leaving silicon whiskers in place at $\rho > 0.95$ due to the nanoporosity of the catalyst film (Figure S2d−g).

We further support our model by modulating the surface crystal plane of the silicon wafer. For both N and P Si, the etch rate and morphology do not depend on the crystal axis (Figure 3), because the Schottky barrier height changes very little with crystal plane.
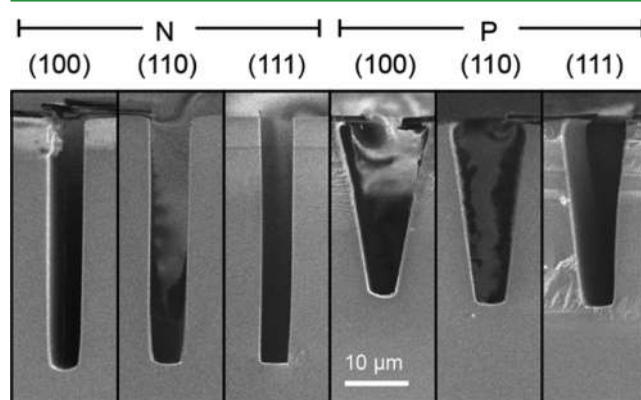

Figure 3. SEM images of the morphology of the MACE reaction after 1 h in a $\rho = 0.4$, $C = 4.8$ M solution for N and P Si for different surface crystal orientations. Scale bar is 10 μm, applicable to all images.

Note that this observation contrasts with the crystal axis dependencies observed with nanoparticle MACE catalysts.[24,25] Our nanoporous film is well-explained by a band diagram, but nanoparticle catalysts may not be explained as such. Other works have explained the crystal axis dependence based on the surface energy differences along different crystal planes of Si.[12,25,26] However, our explanation is consistent with previous studies of doping dependent etch rate using Ag nanoparticles,[11] as well as evidence of hole carrier drift in highly doped n-type Si using Ag and Pt catalysts.[11,27] The etch rate dependence on the catalyst material[12] depends largely on the catalytic reactivity of the metal with H_2O_2, because these catalyst materials have very similar reported Schottky barrier heights.[21,28] Our contribution to the MACE mechanism clarifies the previously mystifying doping dependence of MACE.

To further elucidate the MACE mechanism, we measured the etch rate dependence on the solution composition to obtain kinetic rate exponents, which, to our knowledge, has not yet been measured for this reaction. We fix $\rho = 0.4$, and vary the combined solution concentration of $C = [HF]+[H_2O_2]$. We measure the etch-rate for N Si, and allometrically fit the etch rates with an exponent of 1.62 (Figure 4a). On the basis of the reaction equation, the etch rate scales like the following
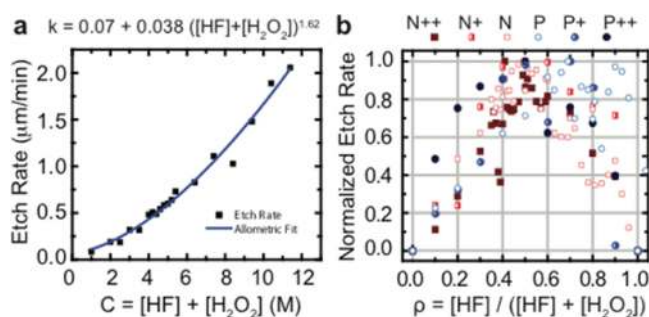
Figure 4. (a) Etch rate for N Si with fixed $\rho = 0.4$, with an allometric fit to the rate, equation shown above. (b) Etch rates for all dopings of Si, normalized to maximum observed rate.

Figure 5. (a) Schematic of the MACE doping etch stop. (b) Cross-section SEM of the etched N Si structure after 5 h in a $\rho = 0.4$, $C = 4.8$ M solution. (c) Detail view SEM of the etch-stop after 5 h. (d) Time dependence of the etch depth.

$$\text{rate} \sim [\text{h}^+]^z [\text{HF}]^x [\text{H}_2\text{O}_2]^y = [\text{h}^+]^z \rho^x (1 - \rho)^y C^{x+y}$$

and so the sum of the kinetic rate exponents for $[\text{HF}]$ and $[\text{H}_2\text{O}_2]$ is 1.62, $x + y = 1.62$. The scaling of the etch rate with C also holds for P+ Si in the range $C = 12.6$ M to $C = 3.1$ M at $\rho = 0.93$, corresponding to an etch rate range of 1.75 to 0.1 μm/min.

We plot the etch rates for a fixed $C = 4.8$ M, normalized to the maximum for each doping type, and observe that as a function of ρ the etch rate maximum occurs near $\rho = 0.5$ for all n-type Si and for P++ Si (Figure 4b). Therefore, for these dopings of Si, the kinetic rate exponents for $[\text{HF}]$ and $[\text{H}_2\text{O}_2]$ must be equal, and $x = y = 0.81$.

For P Si and P+ Si, we observe two maxima. These two maxima correspond to two distinct etch mechanisms. In the regime $\rho < 0.5$, P Si and P+ Si etch with a morphology very similar to that observed in N, N+, N++, and P++ Si. In the regime $\rho > 0.9$, the etch morphology is completely distinct, forming porous Si, with a combined morphology observed in the range $0.5 < \rho < 0.9$ (Figure 1d, Figure S2). The maximum at higher ρ corresponds to porous Si formation by MACE in p-type Si, while the maximum at lower ρ corresponds to solid MACE etching, as also previously observed.[29] Because of the similarity in morphology, and because P+ Si obeys the same scaling with C as N Si, the kinetic exponents for P Si and P+ Si are also likely $x = y = 0.81$.

From the noninteger values of the kinetic exponents, we infer that MACE involves the coparticipation of more than one HF-etching mechanisms, as well as the coparticipation of HF, F$^-$, and HF$_2^-$ in those mechanisms.[29,30] The importance of several mechanisms is consistent with the literature on anodic HF etching of Si and uncatalyzed HF-H$_2$O$_2$ etching of Si.[3,11] For a detailed consideration of the MACE mechanism, see the Supporting Information.

The P++ Si etch rate and N Si etch rate differ by about a factor of 40. We apply this to fabricate a novel doping etch stop for MACE (Figure 5). We fabricate an 8 μm deep P++ Si layer on the backside of an N Si wafer using spin-on-glass (Figure 5a). a). We then pattern the top surface and use MACE to etch the wafer. The etching slows down when the catalyst hits the p-type silicon and etches in a porous fashion (Figure 5b–d), similar to the morphology for p-type silicon shown in Figure 1d.

In summary, we have proposed a novel model of metal-assisted chemical etching of silicon using a nanoporous Au catalyst with an H$_2$O$_2$ oxidant and Si-HF dissolution reaction. The etch rate and morphology of the etching reaction is explained by the Schottky barrier electric field at the interface of the catalyst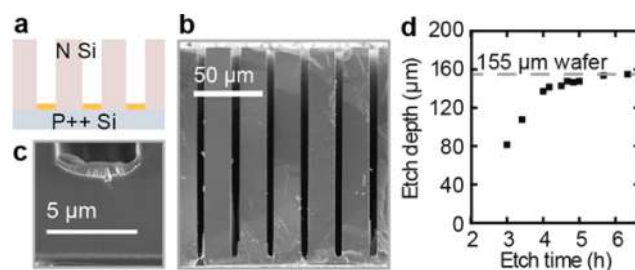 and the silicon. We expect that this understanding will aid in the development of new MACE reactions for other materials and etchants.

■ ASSOCIATED CONTENT

Ⓢ Supporting Information

The Supporting Information is available free of charge on the ACS Publications website at DOI: 10.1021/acsami.6b01020.

> Figures showing various micromachining of silicon using MACE; an expanded version of the morphology matrix in Figure 1; gold morphology after etching; Schottky barrier data; further discussion on mechanism and methods (PDF)

■ AUTHOR INFORMATION

Corresponding Author

*E-mail: yicui@stanford.edu.

Present Address

$^\perp$V.K.N. is currently at Intermolecular, 3011 North First Street, San Jose, CA 95134.

Author Contributions

†R.A.L. and T.M.H. contributed equally.

■ ACKNOWLEDGMENTS

■ REFERENCES

(1) Aachboun, S.; Ranson, P. Deep Anisotropic Etching of Silicon. *J. Vac. Sci. Technol., A* **1999**, *17*, 2270−2273.

(2) Van Olmen, J.; Mercha, A.; Katti, G.; Huyghebaert, C.; Van Aelst, J.; Seppala, E.; Chao, Z.; Armini, S.; Vaes, J.; Teixeira, R. C. 3D Stacked IC Demonstration Using a Through Silicon Via First Approach. *Proceedings of the 2008 Electron Devices Meeting*; IEEE: Piscataway, NJ, 2008; pp 1−4.

(3) Li, X. Metal Assisted Chemical Etching for High Aspect Ratio Nanostructures: A Review of Characteristics and Applications in Photovoltaics. *Curr. Opin. Solid State Mater. Sci.* **2012**, *16*, 71−81.

(4) Narasimhan, V. K.; Hymel, T. M.; Lai, R. A.; Cui, Y. Hybrid Metal-Semiconductor Nanostructure for Ultrahigh Optical Absorption and Low Electrical Resistance at Optoelectronic Interfaces. *ACS Nano* **2015**, *9*, 10590−10597.

(5) Chan, C. K.; Peng, H.; Liu, G.; McIlwrath, K.; Zhang, X. F.; Huggins, R. A.; Cui, Y. High-Performance Lithium Battery Anodes Using Silicon Nanowires. *Nat. Nanotechnol.* **2008**, *3*, 31−35.

(6) Li, X.; Bohn, P. W. Metal-assisted Chemical Etching in HF/H_2O_2 Produces Porous Silicon. *Appl. Phys. Lett.* **2000**, *77*, 2572−2574.

(7) Wu, B.; Kumar, A.; Pamarthy, S. High Aspect Ratio Silicon Etch: A Review. *J. Appl. Phys.* **2010**, *108*, 051101.

(8) Park, J.-H.; Gu, L.; von Maltzahn, G.; Ruoslahti, E.; Bhatia, S. N.; Sailor, M. J. Biodegradable Luminescent Porous Silicon Nanoparticles for *In Vivo* Applications. *Nat. Mater.* **2009**, *8*, 331−336.

(9) Li, Y. Y.; Cunin, F.; Link, J. R.; Gao, T.; Betts, R. E.; Reiver, S. H.; Chin, V.; Bhatia, S. N.; Sailor, M. J. Polymer Replicas of Photonic Porous Silicon for Sensing and Drug Delivery Applications. *Science* **2003**, *299*, 2045−2047.

(10) Steiner, P.; Lang, W. Micromachining Applications of Porous Silicon. *Thin Solid Films* **1995**, *255*, 52−58.

(11) Zhang, M.-L.; Peng, K.-Q.; Fan, X.; Jie, J.-S.; Zhang, R.-Q.; Lee, S.-T.; Wong, N.-B. Preparation of Large-Area Uniform Silicon Nanowires Arrays through Metal-Assisted Chemical Etching. *J. Phys. Chem. C* **2008**, *112*, 4444−4450.

(12) Yae, S.; Morii, Y.; Fukumuro, N.; Matsuda, H. Catalytic Activity of Noble Metals for Metal-Assisted Chemical Etching of Silicon. *Nanoscale Res. Lett.* **2012**, *7*, 352.

(13) Huang, Z.; Geyer, N.; Werner, P.; de Boor, J.; Gösele, U. Metal-Assisted Chemical Etching of Silicon: A Review. *Adv. Mater.* **2011**, *23*, 285−308.

(14) Li, L.; Zhao, X.; Wong, C.-P. Charge Transport in Uniform Metal-Assisted Chemical Etching for 3D High-Aspect-Ratio Micro- and Nanofabrication on Silicon. *ECS J. Solid State Sci. Technol.* **2015**, *4*, P337−P346.

(15) Lai, C. Q.; Cheng, H.; Choi, W. K.; Thompson, C. V. Mechanics of Catalyst Motion During Metal Assisted Chemical Etching of Silicon. *J. Phys. Chem. C* **2013**, *117*, 20802−20809.

(16) Geyer, N.; Fuhrmann, B.; Huang, Z.; de Boor, J.; Leipner, H. S.; Werner, P. Model for the Mass Transport During Metal-Assisted Chemical Etching with Contiguous Metal Films as Catalysts. *J. Phys. Chem. C* **2012**, *116*, 13446−13451.

(17) Wang, D.; Ji, R.; Du, S.; Albrecht, A.; Schaaf, P. Ordered Arrays of Nanoporous Silicon Nanopillars and Silicon Nanopillars with Nanoporous Shells. *Nanoscale Res. Lett.* **2013**, *8*, 42.

(18) Li, L.; Liu, Y.; Zhao, X.; Lin, Z.; Wong, C.-P. Uniform Vertical Trench Etching on Silicon with High Aspect Ratio by Metal-Assisted Chemical Etching Using Nanoporous Catalysts. *ACS Appl. Mater. Interfaces* **2014**, *6*, 575−584.

(19) Lai, C. Q.; Zheng, W.; Choi, W. K.; Thompson, C. V. Metal Assisted Anodic Etching of Silicon. *Nanoscale* **2015**, *7*, 11123−11134.

(20) Crowell, C. R. The Richardson Constant for Thermionic Emission in Schottky Barrier Diodes. *Solid-State Electron.* **1965**, *8*, 395−399.

(21) Turner, M. J.; Rhoderick, E. H. Metal-Silicon Schottky Barriers. *Solid-State Electron.* **1968**, *11*, 291−300.

(22) Smith, B. L.; Rhoderick, E. H. Shcottky Barriers on *p*-type Silicon. *Solid-State Electron.* **1971**, *14*, 71−75.

(23) Chang, C.; Sakdinawat, A. Ultra-High Aspect Ratio High-Resolution Nanofabrication for Hard X-ray Diffractive Optics. *Nat. Commun.* **2014**, *5*, 4243.

(24) Megouda, N.; Hadjersi, T.; Piret, G.; Boukherroub, R.; Elkechai, O. Au-Assisted Electroless Etching of Silicon in Aqueous HF/H_2O_2 Solution. *Appl. Surf. Sci.* **2009**, *255*, 6210−6216.

(25) Huang, Z.; Shimizu, T.; Senz, S.; Zhang, Z.; Geyer, N.; Gösele, U. Oxidation Rate Effect on the Direction of Metal-Assisted Chemical and Electrochemical Etching of Silicon. *J. Phys. Chem. C* **2010**, *114*, 10683−10690.

(26) Liu, G.; Young, K. L.; Liao, X.; Personick, M. L.; Mirkin, C. A. Anisotropic Nanoparticles as Shape-Direction Catalysts for the Chemical Etching of Silicon. *J. Am. Chem. Soc.* **2013**, *135*, 12196−12199.

(27) Chattopadhyay, S.; Li, X.; Bohn, P. W. In-Plane Control of Morphology and Tunable Photoluminescence in Porous Silicon Produced by Metal-Assisted Electroless Chemical Etching. *J. Appl. Phys.* **2002**, *91*, 6134−6140.

(28) de Sousa Pires, J.; d' Heurle, F.; Norde, H.; Petersson, S.; Tove, P. A. Measurements of the Rectifying Barrier Heights of Various Rhodium Silicides with n-Silicon. *Appl. Phys. Lett.* **1980**, *36*, 153−155.

(29) Chartier, C.; Bastide, S.; Lévy-Clément, C. Metal-Assisted Chemical Etching of Silicon in $HF-H_2O_2$. *Electrochim. Acta* **2008**, *53*, 5509−5516.

(30) Lehmann, V. *Electrochemistry of Silicon*; Wiley-VCH Verlag GmbH: Weinheim, FRG, 2002; Vol. 3.